Full characterization of spatial coregistration errors and spatial resolution in spectral imagers

HANS ERLING TORKILDSEN AND TORBJØRN SKAULI*

Norwegian Defence Research Establishment (FFI), P O Box 25, 2007 Kjeller, Norway
**Corresponding author: torbjorn.skauli@ffi.no*

Received XX Month XXXX; revised XX Month, XXXX; accepted XX Month XXXX; posted XX Month XXXX (Doc. ID XXXXX); published XX Month XXXX

For multi- and hyperspectral imagers, the integrity of the spectral information depends critically on the spatial coregistration between bands. There is at present no commonly accepted way to fully specify coregistration performance. This paper shows how a relatively simple measurement technique can be used to form sharp images of the point spread function in all bands, yielding information about spatial coregistration, as well as spatial resolution. A previously proposed metric is applied to characterize coregistration in terms of PSF similarity between bands. Resolution is characterized by ensquared energy. Two commercial hyperspectral cameras with nominally similar specifications are compared, and turn out to have large differences in their actual performance. The results, and the relative simplicity of the measurement, suggest that the method is suitable as a standardized performance test. © 2015 Optical Society of America

OCIS codes: *(110.4234) Multispectral and hyperspectral imaging; (100.4145) Motion, hyperspectral image processing; (220.4840) Testing; (110.3925) Metrics; (110.4100) Modulation transfer function.*

http://dx.doi.org/10.1364/OL.99.099999

Hyperspectral imaging has become a widely used measurement technique, in applications ranging from microscopy to planetary science. It is well recognized that the quality of the spectral signal depends critically on the spatial coregistration of bands, since subsequent processing of a pixel spectrum normally assumes that all bands have the same point spread function (PSF). Commercial hyperspectral cameras are often specified in terms of the "keystone" distortion, essentially the pixel centroid shift resulting from residual wavelength-dependence of magnification. However, this measure of pixel shift does not account for wavelength dependencies in the width or shape of the PSF. Thus there is a very real possibility for hyperspectral cameras with the same coregistration specification to exhibit large differences in their actual coregistration performance.

Several works have considered coregistration beyond the simple keystone measure. In [1], for example, a scanned line source is used to measure the line spread function (LSF) in the "along-track" and "across-track" directions of an imaging spectrometer. The variation of the LSF with wavelength and position in the field of view (FOV) was mapped by using a Gaussian fit to find the LSF position and width, quantities recommended in [2] to guide optical design. Further review and discussion of PSF measurement is given in [3]. In [4] a method is proposed for characterizing coregistration and sharpness in the across-track direction. In [5], a coregistration error metric is proposed and shown to be a generalization of keystone error, while also capturing differences in PSF width and shape. It is proposed to use tomographic reconstruction to measure the full PSF of all bands. In [6], we showed this scheme to be feasible, by characterizing a multispectral camera.

In this letter, we describe the first measurements of the full PSF shape of hyperspectral cameras, using an improved measurement setup which can characterize the coregistration performance accurately in a reasonably short time. We present measurements of coregistration and sharpness for two different, relatively new, commercial hyperspectral cameras. Judging from their specifications, the cameras are comparable, but the measurements reveal large differences in their actual performance.

We use the metric proposed in [5], which is essentially the volume between the PSFs of two bands. For band indices n and m, the spatial coregistration error metric $\varepsilon_{s,nm}$ is an integral of the absolute value of the PSF difference over the image (x,y) plane

$$\varepsilon_{s,nm} = \frac{1}{2}\iint_{x,y} \left| f_m(x,y) - f_n(x,y) \right| \mathrm{d}x\,\mathrm{d}y \qquad (1)$$

where $f_n(x,y)$ is the PSF for band n, normalized to unity integral. The metric value represents an upper bound on the weighting error of spectral components in a mixed pixel containing areas of the scene with different radiance spectra, and can be interpreted as a generalization of keystone error[5]. An overall metric for coregistration performance of a camera can be formed from the mean or maximum value over all band pairs.

Obviously, the PSF shape also provides information about spatial resolution. It is important to characterize resolution together with coregistration, since these will be conflicting goals in imager design[7]. Here we characterize resolution based on the

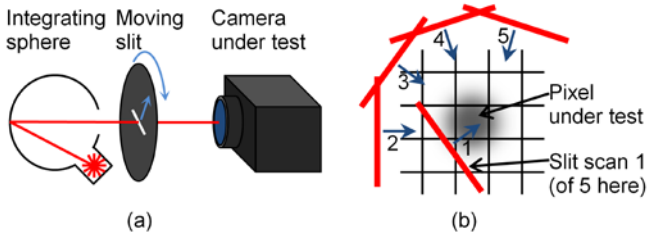

Figure 1. (a) Sketch of the measurement setup. A line source, formed by a slit, is scanned in different directions across part of the field of view. (b) Illustration of the slit scan pattern in the image plane. The slit scans across the PSF of the pixel under test, sequentially in a number of different directions, chosen according to the desired resolution.

mean PSF over all bands. Since hyperspectral image processing most often starts by analyzing individual pixel spectra, rather than spatial contrasts, we characterize resolution by the pixel ensquared energy, evaluated as the fraction of the mean PSF that falls within either the nominal pixel size or the specified instantaneous pixel FOV (IFOV).

To measure the shapes of the PSFs in all bands, and their relative positions, we employ the concept of tomographic scanning imaging[8]. Rather than reconstructing an image of a scene, we use a tomographic technique to form an image of the point spread function. The concept is illustrated in Figure 1. A line source, formed by a slit much narrower than the nominal pixel width in object space, is scanned across part of the field of view of a camera. Here, the cameras were operated at 20 to 100 Hz line rate, and the slit was scanned at a speed of about 1 nominal pixel width per second. The resulting time series recorded from a pixel in a particular band is the line spread function (LSF), for that band. The LSF is a projection of the PSF in a direction orthogonal to the scan direction. By making linear scans in different directions around the circle, a set of PSF projections is obtained, from which the two-dimensional PSF for each band is recovered by an inverse Radon transform. With N scan steps across a pixel, and M different scan directions, the transform produces an image of the PSF resolved in $\approx N \times M$ pixels.

The experimental setup is basically a 22 µm×25 mm slit mounted on a translation stage, which in turn is mounted on a rotation stage and arranged such that the slit scans across a 25mm optical port in the center of rotation. The slit is illuminated from the back by a 5 cm integrating sphere illuminated by halogen lamps (2x20W), supplemented by LEDs at 405 and 420 nm to increase signal in the blue end of the spectrum. The measurement requires some degree of care, such as avoiding mechanical backlash, but no extraordinary experimental effort is needed.

Depending on the magnification and pixel size of the camera, the scanned region is typically several pixels across. To test coregistration variation across the full FOV, it is necessary to repeat the measurement after rotating the camera so that the scanning slit is seen in different parts of the FOV.

Here we show measurement results for two hyperspectral transmission-grating spectrometer cameras, normally used in a line-scanning configuration. Here, the cameras are stationary, so that there is no PSF broadening due to scan motion. Both cameras cover the spectral range from 400 to 1000 nm, approximately. The first camera is a SpecIm PFD camera with 1312 pixels across the FOV, dating from 2012, using an OLE23 23 mm objective lens with adjustable focus. The slit width is 30 µm, imaged 1:1 onto detector

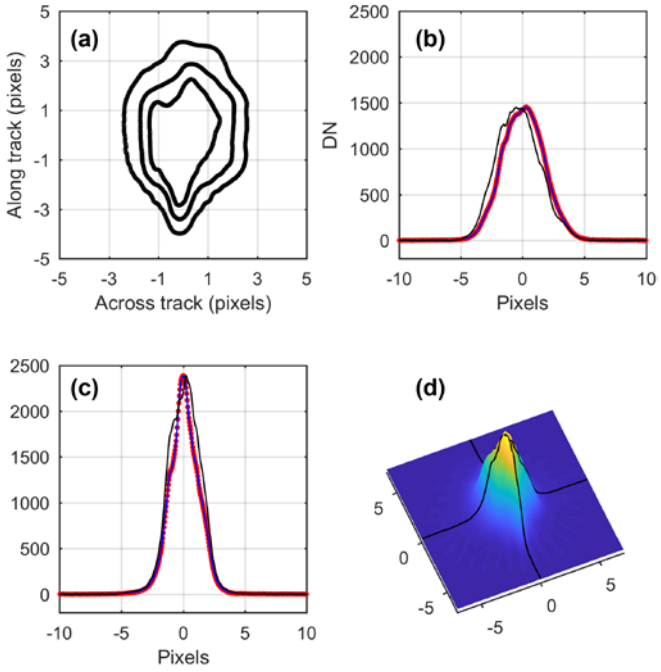

Figure 2. Example of a measured PSF, from the SpecIm camera at 699 nm wavelength. (a) Contour map of the PSF with coutours at 50, 75 and 90% enclosed energy. (b) and (c) Measured line spread function and cross section in the along (b) and across (c) track directions(red). Also shown are line spread functions calculated back from the reconstructed PSF (blue), as well as cross sections through the peak (black). (d) 3D plot of the PSF.

pixels with 8 µm pitch. Thus, the nominal pixel size is 8×8 µm in the spectrometer slit plane, and the specification implies an IFOV of 1 pixel across and 30/8=3.75 pixels along track. The second camera is a HySpex VNIR-1800 camera with 1800 pixels, dating from 2016, using a 1 m fixed focus lens. This camera has a specified IFOV of 1×2 pixels. Focus was adjusted by translating the camera.

The measurements presented here were recorded near the center of the field of view for each of the two cameras. The cameras were viewing the slit at a distance of 1 m. (Alternatively, the slit could be placed in the source plane of a collimator, to test cameras focused at infinity.) Except where noted, the cameras were focused by optimizing the ensquared energy in a nominal square pixel.

Figure 2 shows an example of a measured PSF. Next to the contour map (a), the directly measured LSF is shown in the along (b) and across (c) track directions, together with an LSF calculated from the reconstructed PSF. Also shown is a cross section through the peak of the PSF in each direction. The 3D image (d) of the reconstructed PSF shows that there is some noise and artifacts in the region of near-zero response outside the main PSF peak. Artifacts from the reconstruction have been reduced by spectral filtering in the tangential direction, after transformation to cylindrical coordinates. The remaining noise and artifacts in the signal away from the peak will tend to average out to zero. However, if the metric integral (1) includes these areas, the coregistration error will be overestimated. To minimize the contribution of noise, a threshold is set for the PSF in each band, so that 95% of the PSF energy is above the threshold. The metric integral (1) is then evaluated over the area where both PSFs are above their respective thresholds. With this procedure, the estimated coregistration error reflects the differences between

Dette er en postprint-versjon / This is a postprint version.
DOI til publisert versjon / DOI to published version: 10.1364/OL.43.003814

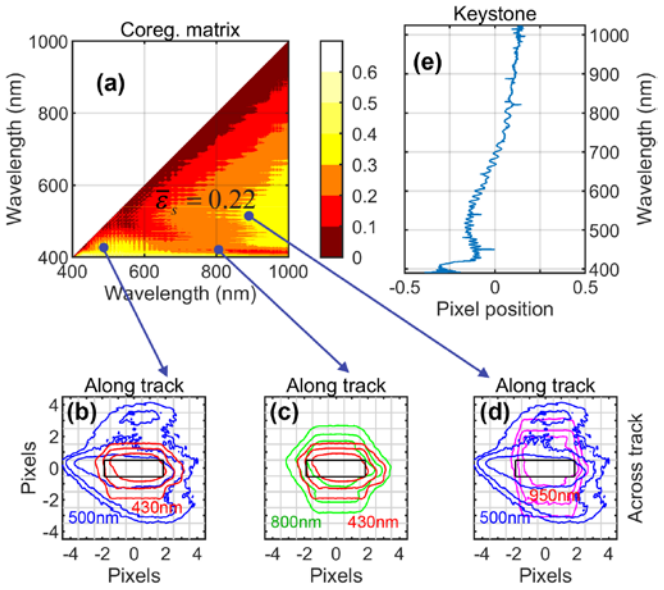

Figure 3. Results from the SpecIm PFD camera. (a) The matrix $\varepsilon_{s,nm}$ of coregistration error between all band pairs. (b)-(d) Selected PSFs from pairs of wavelengths as shown. Contours enclose 50, 75 and 90% of PSF energy. The black rectangle is the specified pixel IFOV. (e) Wavelength dependence of "keystone" positional offset, calculated from PSF centroid in each band. See also Visualization 1.

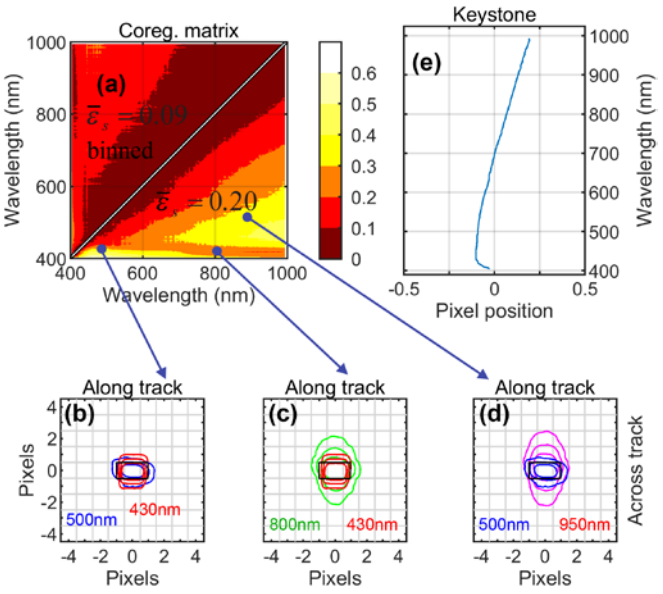

Figure 4. Results from the HySpex VNIR-1800 camera. (a) The matrix $\varepsilon_{s,nm}$ of coregistration error between all band pairs. Lower half: full resolution. Upper half: 3×3 binning for comparison, see text. (b)-(d) Selected PSF pairs, plotted as for Figure 3. (e) Wavelength dependence of "keystone" positional offset, calculated from PSF centroid in each band. See also Visualization 2.

PSFs in the main peak. If the threshold is set lower, to include more of the PSF, we observe an increase in metric values, evidently due to contributions from noise and artifacts. The PSF truncation discards effects of wavelength-dependent stray light, which may be an important aspect of imager performance, but represents only a small fraction of PSF energy, and should be described in terms of other characteristics than coregistration error. The truncated parts of the PSF will normally contribute significantly less than 0.05 to the metric value, which in turn is well below the observed values. Thus truncation will have a relatively small effect.

Figure 3 shows measured results for the SpecIm PFD camera. The matrix of measured coregistration error values for each band pair is shown as a colored contour plot in (a). (Only data below the diagonal are shown, since $\varepsilon_{s,nm} = \varepsilon_{s,mn}$.) The mean coregistration error over all band pairs is 0.22, 90% of values are below 0.35 and the maximum is 0.78. Figure 3 (b) to (d) show contour plots of a few pairs of PSFs corresponding to different points in the matrix in (a), illustrating how the data in the matrix arise. Visualization 1 shows the PSF evolution with wavelength. For the sharper PSFs in (c), an elongation due to the slit width is clearly seen, consistent with the specified pixel IFOV, but generally the PSF is significantly larger. The peak ensquared energy within a single pixel is 7% of the mean PSF, but within the specified pixel IFOV of 1x3.75 pixels, the ensquared energy is 19%.

The data in Figure 3 (a) exhibit two maxima (lighter colours), because the largest coregistration errors occur between the middle and the ends of the spectral range, coarsely speaking. This behavior is reasonable, since the shape of the PSF will tend to change gradually across the spectral range. The PSF exhibits an oscillatory variation with increasing period towards longer wavelength, leading to the periodic variations seen in the data. This is a real effect, and not due to noise or artifacts in the measurement. The periodicity corresponds to etalon interference in a 13 μm air gap. Thus the periodic variations in (a) are likely due to modulation of the PSF shape by an etalon located in a convergent beam somewhere in the spectrometer optics.

Figure 3 (e) shows how the across-track position of the PSF centroid varies with wavelength, *i.e.* the conventional measure of keystone. The centroid position spans a range of about 0.5 pixels. This could be specified as a keystone error of +/-0.25 pixels, and is less than the mean value of ε_s, and well below the maximum value 0.78. Thus a large part of the total coregistration error is due to PSF shape differences, illustrating how keystone fails to capture the full range of coregistration errors.

Figure 4 shows measured results for the HySpex VNIR-1800 camera. The lower part of Figure 4 (a) shows the coregistration error when the camera is focused and operated normally, for maximum ensquared energy. Then the mean coregistration error is 0.20, 90% of values are below 0.36, and the maximum is 0.60. Contour plots in Figure 4 (c) to (d) show pairs of PSFs from different wavelengths on the same scale as in Figure 3. It can be seen that the width of the PSF is significantly narrower for this camera, and closer to the specification. The peak ensquared energy within a single pixel is 35% of the mean PSF. Within the nominal pixel FOV of 1×2 pixels, the ensquared energy is 56%.

The overall behavior of the coregistration error matrix is qualitatively similar to that in Figure 3, due to gradual change of PSF with wavelength, as shown in Visualization 2. No oscillatory behavior of the PSF is seen. The centroid plot in Figure 4 (e) shows a variation equivalent to ±0.15 pixel keystone error, well below the mean and max of ε_s. Thus again we find that keystone fails to capture the full coregistration error.

To illustrate the tradeoff between coregistration and resolution, the upper part of Figure 4 (a) shows measured coregistration errors when the HySpex camera image is binned 3×3, synthesized

Dette er en postprint-versjon / This is a postprint version.
DOI til publisert versjon / DOI to published version: 10.1364/OL.43.003814

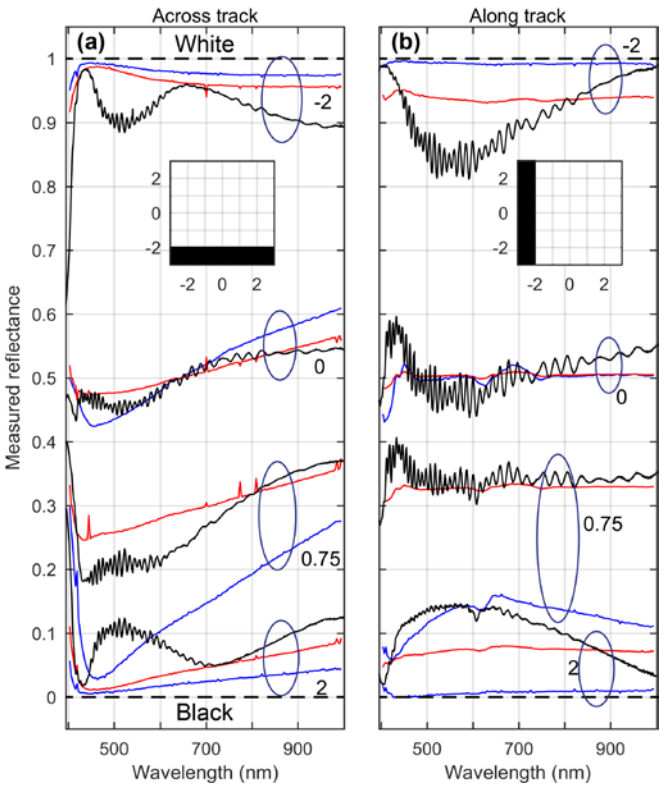

Figure 5. Spectra that would be recorded near a black-white edge, calculated from the measured PSFs. Black lines: SpecIm camera. Blue: HySpex camera. Red: HySpex 3x3 binned pixel. Numbers indicate edge position relative to pixel center for the indicated groups of graphs. Insets show edges at position -2 pixels. a) Edge oriented in the along-track direction, in different cross-track positions. b) As for a) with an edge in the cross-track direction. See Visualization 3.

from the measured PSF. Then the PSF width is nearly as large as the SpecIm camera. In this setting, the mean coregistration error is 0.09, 90% of values are below 0.16, and the maximum is 0.27. The ensquared energy within the nominal binned pixel is 81%. Alternatively, the resolution could be made comparable by moving the HySpex camera out of focus to make the ensquared energy equal to that of the SpecIm camera. In this setting we measured coregistration values comparable to those found with 3×3 binning.

To illustrate the effect of coregistration errors on image data, consider the practically important case of a scene containing an edge between bright and dark areas. Taking as example an edge between black and white uniform areas, it is clear that reflectances estimated from pixels near the edge should ideally be spectrally gray. The effect of scanning such an edge through the pixel can be simulated based on our measured PSF data. Example results are shown in Figure 5. It can be seen that both cameras produce significant spectral artifacts near the edge. However, the HySpex camera exhibits a quicker transition from white to black, due to its sharper PSF, and thus overall produces less distortion of image data. The figure also shows the spectra that would be produced by the HySpex camera with the binning scheme mentioned above. These spectra still exhibit spectral artifacts, but are noticeably flatter than those that would be produced by the SpecIm camera.

Note that although the results in the figure are simulated from our measurement of PSF shape, the same spectra could be measured directly, by translating a knife edge in front of a uniform light source, or by a single slit scan. Such measurements could be made with a simpler experimental setup, and could form the basis of a simplified coregistration testing scheme, but many forms of coregistration error would then be missed. A better alternative would be a direct PSF measurement by 2D scanning of a point source based on recently available broadband laser sources.

The cameras tested here are comparable in the sense that their main characteristics are similar, and they target the same applications and market segments. However, the purpose of this work is not to make a comparative review of the cameras, which would involve several other characteristics in addition to coregistration and resolution. We point out that the camera which is found to be better is also several years newer than the other, and no effort has been made to ensure that the tested units are representative ones. What is clearly shown by the results is that there may be very large differences between commercial hyperspectral cameras, which are not adequately reflected in the way such cameras are specified today. This is consistent with the general need for improved standards and techniques for characterization of spectral imagers[9]. This work has demonstrated the feasibility of detailed measurement of PSF shape using a relatively simple experimental setup. The measurement technique and coregistration metric are applicable or adaptable to a wide range of spectral camera architectures. The measured data provide full information about spatial coregistration and resolution. A variety of performance metrics can be extracted from these data. We propose the metric (1) and the ensquared energy in the specified IFOV as preferable, measurable, conservative and meaningful metrics for spatial coregistration and resolution in spectral imaging.

Acknowledgments. The authors are grateful to Ingunn Burud and Espen Olsen of the Norwegian University of Life Sciences for lending us the SpecIm camera for testing, and to Harald Hovland and Thomas Opsahl for advice on processing PSF measurements. This work is based on results presented at SPIE DCS 2018 in paper 10644-51.

Disclosures. FFI has ongoing collaborations with NEO, makers of the HySpex camera. The work presented here, however, has been carried out independently by FFI. The HySpex camera has been purchased by FFI on commercial terms following a public tender.

References

1. Karim Lenhard, Andreas Baumgartner, and Thomas Schwarzmaier, IEEE Trans. Geosci. Remote Sens. **53**, 1828-1841 (2015)
2. Lori B. Moore and Pantazis Mouroulis, Proc. SPIE **10590**, 105900Q (2017)
3. Jurij Jemec, Franjo Pernuš, Boštjan Likar, and Miran Bürmen, Int. J. Comput. Vis. **121**, 391-402 (2017)
4. Gudrun Høye, Trond Løke, and Andrei Fridman, Opt. Eng. **54**, 053102 (2015)
5. Torbjørn Skauli, Opt. Express **20**, 918-933 (2012).
6. Hans Erling Torkildsen, Harald Hovland, Thomas Opsahl, Trym Vegard Haavardsholm, Stéphane Nicolas, and Torbjørn Skauli, Proc. SPIE **9088**, 908819 (2014)
7. Torbjørn Skauli, Appl. Opt. **52**, C58-C63 (2013)
8. Hovland, Harald, Opt. Expr. **17**, 11371-11387 (2009)
9. Torbjørn Skauli, Proc. SPIE **10213**, 102130H (2017)

DOI til publisert versjon / DOI to published version: 10.1364/OL.43.003814